

Observation of a two-dimensional spin-lattice in non-magnetic semiconductor heterostructures

Christoph Siegert,¹ Arindam Ghosh,^{1,2,*} Michael Pepper,¹ Ian Farrer,¹ and David A. Ritchie¹

¹*Cavendish Laboratory, University of Cambridge,*

J.J. Thomson Avenue, Cambridge CB3 0HE, United Kingdom.

²*Department of Physics, Indian Institute of Science, Bangalore 560 012, India.*

(Dated: October 10, 2018)

Tunable magnetic interactions in high-mobility nonmagnetic semiconductor heterostructures are centrally important to spin-based quantum technologies. Conventionally, this requires incorporation of “magnetic impurities” within the two-dimensional (2D) electron layer of the heterostructures, which is achieved either by doping with ferromagnetic atoms [1], or by electrostatically printing artificial atoms or quantum dots [2, 3, 4, 5]. Here we report experimental evidence of a third, and intrinsic, source of localized spins in high-mobility GaAs/AlGaAs heterostructures, which are clearly observed in the limit of large setback distance (≈ 80 nm) in modulation doping. Local nonequilibrium transport spectroscopy in these systems reveal existence of multiple spins, which are located in a quasiregular manner in the 2D Fermi sea, and mutually interact at temperatures below 100 millikelvin via the Ruderman-Kittel-Kasuya-Yosida (RKKY) indirect exchange. The presence of such a spin-array, whose microscopic origin appears to be disorder-bound, simulates a 2D lattice-Kondo system with gate-tunable energy scales.

Unintentional magnetic impurities are expected to be absent in high-quality nonmagnetic semiconductors, such as molecular beam epitaxy-grown GaAs/AlGaAs heterostructures. Contrary to this general belief, recent observation of a Kondo-like resonance in low-energy density-of-states of one dimensional (1D) quantum wires indicated existence of localized spin in mesoscopic GaAs/AlGaAs-based devices [6]. Subsequently, evidence of localized spins was also reported in unconfined quasi-ballistic 2D systems [7, 8], instigating the question whether localized spins are intrinsic to GaAs/AlGaAs-based nonmagnetic semiconductors, and if so, what is the microscopic origin of these spins. A fascinating aspect of this problem is the possibility of a layer of mutually interacting spins: a system of considerable importance in studying various forms of magnetic ordering, quantum phase transitions and non-Fermi liquid effects (see Ref. [9] for a review).

In the past experiments with ballistic 1D or 2D systems [6, 7, 8], localized spins were detected with nonequilibrium transport spectroscopy. Pronounced structures, commonly known as zero-bias anomaly (ZBA),

in differential conductance (dI/dV) of mesoscopic devices close to zero source-to-drain electric potential (V_{SD}) were interpreted to be a consequence of spin-spin or spin-conduction electron exchange interaction. Here, we have augmented the nonequilibrium transport spectroscopy with perpendicular-field magnetoresistance measurements, which not only confirm the existence of multiple localized spins within high-mobility GaAs/AlGaAs heterostructures, but also reveals a striking order in the spatial distribution of these spins that becomes visible over a narrow range of n_{2D} .

Mesoscopic devices fabricated from Si monolayer-doped GaAs/AlGaAs heterostructures were used, where the 2D electron layer was formed 300 nm below the surface. A thick (≈ 80 nm) spacer layer of undoped AlGaAs between the dopants and the electrons provided a heavily compensated dopant layer with a filling factor $f \approx 0.9$. The resulting high electron mobility ($\sim 1-3 \times 10^6$ cm²/V-s) provides a long as-grown elastic mean free path $\sim 6-8$ μ m, which acts as an upper limit to the device dimensions, ensuring quasi-ballistic transport. (Micrograph of a typical device is shown in Fig. 1a.)

At low electron temperatures ($T \lesssim 100$ mK) and zero magnetic field, both equilibrium and nonequilibrium transport display rich structures well up to linear conductance $G \sim 10 - 15 \times (e^2/h)$, as the voltage V_G on the gate is increased. For most devices the structures are strongest at carrier density $n_{2D} \sim 1 - 3 \times 10^{10}$ cm⁻² (Fig. 1b), and consist of a repetitive sequence of two-types of resonances at the Fermi energy (E_F). This is illustrated in the surface plot of dI/dV in Figs. 1c for device 1 of Fig. 1a. We denote the strong single-peak resonance at $V_{SD} = 0$ as ZBA-I, which splits intermittently to form a double-peaked ZBA with a gap at E_F , henceforth referred to as ZBA-II. The illustrations of ZBA-I and ZBA-II in the inset of Fig. 1c were recorded at points I and II in Fig 1b, respectively. We define Δ as the half-width at half-depth of ZBA-II. While similar nonequilibrium characteristics was observed in over 50 mesoscopic devices from 5 different wafers, reducing the setback distance below $\sim 60 - 80$ nm was generally found to have detrimental effect on the clarity of the resonance structures (for both ZBA-I and ZBA-II), often leading to broadening or complete suppression.

The nature of suppression of such low-energy resonances with increasing T and at finite in-plane magnetic

field ($B_{||}$) indicate Kondo-like exchange (Figs. 1d-1g) [8], and hence presence of localized moments. A complete description can be obtained with the so-called “two impurity” Kondo model, which embodies the interaction of an ensemble of localized spins within the sea of conduction electrons [10, 11, 12, 13, 14, 15]. (See Ref. [8] and Supplementary Information for arguments against alternative explanation of the ZBA.) In the presence of anti-ferromagnetic coupling of individual spins to surrounding conduction electrons, the zero-field splitting of the Kondo-resonance (ZBA-II) arises due to a V_G -dependent, oscillatory inter-impurity exchange J_{12} , leading to the gap $\Delta \sim |J_{12}|$ at E_F . At certain intermediate values of V_G one obtains ZBA-I when $|J_{12}| \ll k_B T$. For ZBA-II, nonzero J_{12} results in a nonmonotonic suppression of dI/dV at low bias ($|V_{SD}| \lesssim \Delta$, as indeed observed experimentally (Figs. 1e and 1g), while for ZBA-I this decrease is monotonic, and reflects suppression of single-impurity Kondo-resonance at individual noninteracting spins (see Figs. 1d and 1f) [8].

Mesoscopic devices showing clear resonances in the nonequilibrium transport also display a characteristic linear magnetoresistance (MR) over the same range of n_{2D} , when a small magnetic field (B_{\perp}) is applied *perpendicular* to the plane of 2D electron layer. As shown for a different device, at high T ($\cong 1.4$ K), the MR consists of small peak-like structures at specific values of B_{\perp} superposed on a parabolically increasing background (Fig. 2d), while at low T ($\cong 30$ mK), the magnetotransport breaks into quasi-periodic oscillations irrespective of the structure of the ZBA (Fig. 2a and 2b). We note that both these evidences indicate electron transport in a mesoscopic, quasi-regular array of *antidots*, which has been studied extensively in artificially fabricated antidot-lattices [16, 17, 18]. In the classical regime (high T), the peaks in MR correspond to commensurable cyclotron orbits enclosing fixed number of antidots [16], while at low T , quantum interference leads to the phase coherent oscillations in magnetoconductance, arising from transport along multiple connected Aharonov-Bohm rings as the inelastic scattering length exceeds sample dimensions [17].

The magnetotransport data shown in Fig. 2 allows an estimation of the inter-antidot distance R . In Fig. 2d, on subtracting the background, signature of commensurable orbits at $B_{\perp} \approx 0.08, 0.05$ and 0.03 T corresponding to cyclotron radius of the electron encircling one, two and four antidots respectively (see inset). While this gives $R \sim 500$ nm (using the $n_{2D} \approx 1.31 \times 10^{10}$ cm $^{-2}$), a more accurate estimate of R was obtained by Fourier transforming the low-T phase-coherent oscillations of Fig. 2a and 2b. In Fig. 2c, the power spectra calculated over the range 0 to 0.065 T at both values of V_G show a strong peak at the frequency $f_{\Delta B} \approx eR^2/h \approx 105 \pm 10$ T $^{-1}$, corresponding to one flux quantum through unit cell of the antidot lattice (orbit b). This gives $R \approx 670 \pm 30$ nm,

which is consistent with the estimate from commensurability effect. Satellite peaks often appears in the power spectra, for example those at $f_{\Delta B} \cong 190$ T $^{-1}$ (orbit c) and 50 T $^{-1}$ (orbit a), which can be associated to specific stable orbits as indicated in the inset of Fig. 2a. R was found to be weakly device-dependent, varying between 600 – 800 nm, but insensitive to the lithographic dimensions of the devices.

Collectively, the observed nonequilibrium characteristics and low-field MR results indicate formation of a quasi-regular 2D spin-lattice embedded within the Fermi sea, where apart from the Kondo-coupling, the conduction electrons would also undergo potential scattering at the lattice sites. The nature of such potential scattering can be cotunneling [12], or scattering off the tunnel barrier at the localized sites [19]. In this framework, the RKKY exchange between the spins naturally leads to an oscillatory behavior of J_{12} , where range function $\Psi(2k_F R)$ in the interaction magnitude reverses its sign with a periodicity of π in $2k_F R$, $k_F = \sqrt{2\pi n_{2D}}$ being the Fermi wave vector. Analytically [20],

$$\Delta \sim |J| \sim E_F (J\rho_{2D})^2 |\Psi(2k_F R)| \quad (1)$$

where ρ_{2D} is the 2D density of states and J is the exchange coupling between an impurity spin and local conduction electron. Fig. 3a shows the direct confirmation of this, where we have plotted Δ as a function of $2k_F R$ for the device in Fig. 1c. The clear periodicity of $\approx \pi$ (within $\pm 5\%$) in $2k_F R$ can be immediately recognized as the so-called “ $2k_F R$ -oscillations” in the RKKY interaction, establishing the spin-lattice picture.

The absolute magnitude of J_{12} , and hence Δ , for a 2D distribution of spins may differ widely from the simple two-impurity RKKY interaction, and would be affected by frustrated magnetic ordering or spin glass freezing [21], as well as deviation from perfect periodicity in the spin arrangements [22]. Nevertheless, a framework for relative comparison of Δ in different samples can be obtained from Eq. 1 by normalizing Δ with E_F . As shown in Fig. 3b, adjusting for the experimental uncertainty in k_F and R , Δ/E_F for four different devices with various lithographic dimensions can be made to collapse on the solid line proportional to modulus of pairwise RKKY range function over a wide range of $2k_F R$ [20].

With known inter-spin distance, we shall now discuss two outstanding issues of this paper: (1) the microscopic origin of the uniform array of antidots, and subsequently, (2) emergence of the localized spins. A structurally intrinsic origin of antidots in 2D Fermi sea of modulation-doped high-mobility GaAs/AlGaAs heterostructures can arise from long-range potential fluctuations in the conduction band. Direct experimental imaging of disorder in similar systems reported typical distance between fluctuation to be $\sim 0.5 - 1$ μm , in excellent agreement to the magnitude of R in our devices [23]. In presence of

strong correlation in the dopant layer at large f , theoretical investigations have also indicated a well-defined length scale in the spatial distribution of the potential fluctuations [24].

A disorder-templated localized moment formation can then be envisaged through local depletion of electrons, analogous to moment formation in metal-semiconductor Schottky barriers [19]. We discuss this on the basis of three common representations of disorder and screening in high-mobility GaAs/AlGaAs systems, as schematized in Fig. 4a-c [25]. At high n_{2D} , the background disorder is linearly screened at all points, with local charge fluctuations $|\delta n_{2D}| \ll \langle n_{2D} \rangle$ (Fig. 4a). With decreasing n_{2D} , linear screening will break down *locally* at the maxima of slow potential fluctuations, where n_{2D} becomes smaller than the local (rapid) density fluctuations of the dopants, resulting in the formation of single-particle localized states. Assuming a random distribution of the dopants, this is expected to occur at $n_{2D}^c \sim [(1-f)n_\delta/\pi]^{1/2}/\xi$, where $n_\delta = 2.5 \times 10^{12} \text{ cm}^{-2}$ is the bare dopant density in our devices, and ξ is the localization length. From $f_{\Delta B}$ of orbit a in Fig. 2a we estimate $\xi \sim 150 \text{ nm}$, which gives $n_{2D}^c \approx 1.9 \times 10^{10} \text{ cm}^{-2}$, which indeed marks the onset of strong ZBA (see Fig. 1b).

On further lowering of n_{2D} , the system crosses over to the strongly localized regime ($G \ll e^2/h$), and the 2D electron system disintegrates into puddles, which are often interconnected through quantum point contacts (Fig. 4c). While local spins can form at the point contacts [6, 26], the commensurability effect and phase-coherent magnetoconductance oscillations shown in Fig. 2 cannot be explained in such a picture, as they require extended and uninterrupted electron orbits.

Our experiments thus outline a new microscopic mechanism of local moment formation in high-mobility GaAs/AlGaAs-based semiconductors with remote modulation doping. This has serious implications on the possibility of a gate-tunable *static* spontaneous spin polarization in mesoscopic devices at low temperatures, and hinged on the Kondo-coupling of the localized moments to the surrounding conduction electrons. To verify such a coupling, we have estimated the ratio ϵ/Γ for localized states using experimentally observed Kondo temperature T_K , and that $T_K \sim (E_F/k_B) \exp(\pi\epsilon/2\Gamma)$ in the $U \rightarrow \infty$ limit, where ϵ and Γ are the energy of single-electron state (with respect to E_F), and level broadening respectively (Fig. 4b), and $U \sim e^2/\xi \gg E_F$, is the on-site Coulomb repulsion. Taking the measured $T_K \approx 265 \text{ mK}$ at ZBA-I at point I in Fig. 1c as an example, we find $\epsilon/\Gamma \approx -2.1$, which confirms the Kondo regime.

magnetic. *Science* **281**, 951-956 (1998).

- [2] Goldhaber-Gordon, D. *et al.* Kondo effect in a single-electron transistor. *Nature* **391**, 156-159 (1998).
- [3] Cronenwett, S. M., Oosterkamp, T. H., Kouwenhoven, L. P. A Tunable Kondo Effect in Quantum Dots. *Science* **281**, 540-544 (1998).
- [4] Jeong, H., Chang, A. M., Melloch, M. R. The Kondo Effect in an Artificial Quantum Dot Molecule. *Science* **293**, 2221-2223 (2001).
- [5] Craig, N. J. *et al.* Tunable Nonlocal Spin Control in a Coupled-Quantum Dot System. *Science* **304**, 565-567 (2004).
- [6] Cronenwett, S. M. *et al.* Low-Temperature Fate of the 0.7 Structure in a Point Contact: A Kondo-like Correlated State in an Open System. *Phys. Rev. Lett.* **88**, 226805 (2002).
- [7] Ghosh, A., Ford, C. J. B., Pepper, M., Beere, H. E., Ritchie, D. A. Possible Evidence of a Spontaneous Spin Polarization in Mesoscopic Two-Dimensional Electron Systems. *Phys. Rev. Lett.* **92**, 116601 (2004).
- [8] Ghosh, A. *et al.* Zero-Bias Anomaly and Kondo-Assisted Quasiballistic 2D Transport. *Phys. Rev. Lett.* **95**, 066603 (2005).
- [9] Stewart, G. R. Non-Fermi-liquid behavior in d- and f-electron metals. *Rev. Mod. Phys.* **73**, 797-855 (2001).
- [10] Jayaprakash, C., Krishnamurthy, H. R., Wilkins, J. W. Two-Impurity Kondo Problem. *Phys. Rev. Lett.* **47**, 737-740 (1981).
- [11] Affleck, I., Ludwig, A. W. W. Exact critical theory of the two-impurity Kondo model. *Phys. Rev. Lett.* **68**, 1046-1049 (1992).
- [12] Pustilnik, M., Glazman, L. I. Kondo Effect in Real Quantum Dots. *Phys. Rev. Lett.* **87**, 216601 (2001).
- [13] Vavilov, M. G., Glazman, L. I. Transport Spectroscopy of Kondo Quantum Dots Coupled by RKKY Interaction. *Phys. Rev. Lett.* **94**, 086805 (2005).
- [14] Golovach, V. N., Loss, D. Kondo effect and singlet-triplet splitting in coupled quantum dots in a magnetic field. *Europhys. Lett.* **62**, 83-89 (2003).
- [15] Hofstetter, W., Schoeller, H. Quantum Phase Transition in a Multilevel Dot. *Phys. Rev. Lett.* **88**, 016803 (2002).
- [16] Weiss, D. *et al.* Electron pinball and commensurate orbits in a periodic array of scatterers. *Phys. Rev. Lett.* **66**, 2790-2793 (1991).
- [17] Schuster, R., Ensslin, K., Wharam, D., Khn, S., Kotthaus, J. P. Phase-coherent electrons in a finite antidot lattice. *Phys. Rev. B* **49**, 8510-8513 (1994).
- [18] Weiss, D. *et al.* Quantized periodic orbits in large antidot arrays. *Phys. Rev. Lett.* **70**, 4118-4121 (1993).
- [19] Wolf, E. L., Losee, D. L. Spectroscopy of Kondo and Spin-Flip Scattering: High-Field Tunneling Studies of Schottky-Barrier Junctions. *Phys. Rev. B* **2**, 3660-3687 (1970).
- [20] Béal-Monod, M. T. Ruderman-Kittel-Kasuya-Yosida indirect interaction in two dimensions. *Phys. Rev. B* **36**, 8835-8836 (1987).
- [21] Hirsch, M. J., Holcomb, D. F., Bhatt, R. N., Paalanen, M. A. ESR studies of compensated Si:P,B near the metal-insulator transition. *Phys. Rev. Lett.* **68**, 1418-1421 (1992).
- [22] Roche, S., Mayou, D. Formalism for the computation of the RKKY interaction in aperiodic systems. *Phys. Rev. B* **60**, 322-328 (1999).
- [23] Finkelstein, G., Glicofridis, P. I., Ashoori, R. C.,

* Electronic address: arindam@physics.iisc.ernet.in

[1] Ohno, H. Making Nonmagnetic Semiconductors Ferro-

- Shayegan, M. Topographic Mapping of the Quantum Hall Liquid Using a Few-Electron Bubble. *Science* **289**, 90-94 (2000).
- [24] Grill, R., Döhler, G. H. Effect of charged donor correlation and Wigner liquid formation on the transport properties of a two-dimensional electron gas in modulation δ -doped heterojunctions. *Phys. Rev. B* **59**, 10769-10777 (1999).
- [25] Efros, A. L., Pikus, F. G., Burnett, V. G. Density of states of a two-dimensional electron gas in a long-range random potential. *Phys. Rev. B* **47**, 2233-2243 (1993).
- [26] Graham, A. C., Pepper, M., Simmons, M. Y., Ritchie, D. A., Anomalous spin-dependent behaviour of one-dimensional subbands. *Phys. Rev. B* **72**, 193305 (2005).

Acknowledgement: We acknowledge discussions with C. J. B. Ford, G. Gumbs, M. Stopa, P. B. Littlewood, H. R. Krishnamurthy, B. D. Simons, C. M. Marcus, D. Goldhaber-Gordon and K. F. Berggren. The work was supported by an EPSRC funded project. C.S. acknowledges financial support from Gottlieb Daimler- and Karl Benz-Foundation.

Siegert et al

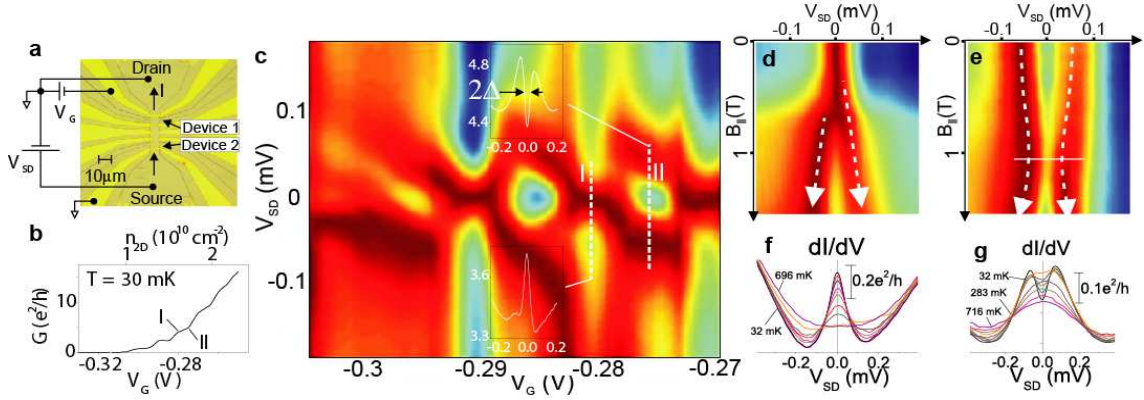


FIG. 1: Nonequilibrium characteristics: **a**, Picture of a set of two typical devices and electrical connections. Active area of a device is defined by the gate-covered region of the etched mesa. The data shown here was obtained from device 1, with device 2 and other side-gates kept grounded. **b**, Typical linear conductance, G , vs. gate voltage V_G (and electron density n_{2D}) for device 1 at 30 mK and zero external magnetic field. **c**, Surface plot of differential conductance dI/dV of device 1 in $V_{SD} - V_G$ plain. Each $dI/dV - V_{SD}$ trace at a particular V_G was vertically shifted for leveling. The insets illustrate ZBA-I and ZBA-II-type resonances at points I and II in Fig. 1b, respectively. **d**, Surface plot of ZBA-I in in-plane magnetic field ($B_{||}$). The dashed line shows a linear monotonic splitting with effective g -factor $|g^*| \approx 0.5$, which confirms the role of spin. **e**, Surface plot of ZBA-II in $B_{||}$. The single-impurity Kondo-behavior dominates above $B_{||} \sim \Delta/g^* \mu_B$ (the horizontal line), where Δ is the half-gap defined in text. **f**, Monotonic temperature (T) suppression of ZBA-I. **g**, T -dependence of dI/dV at ZBA-II. dI/dV is nonmonotonic in T for $|V_{SD}| \lesssim \Delta$.

Siegert et al.

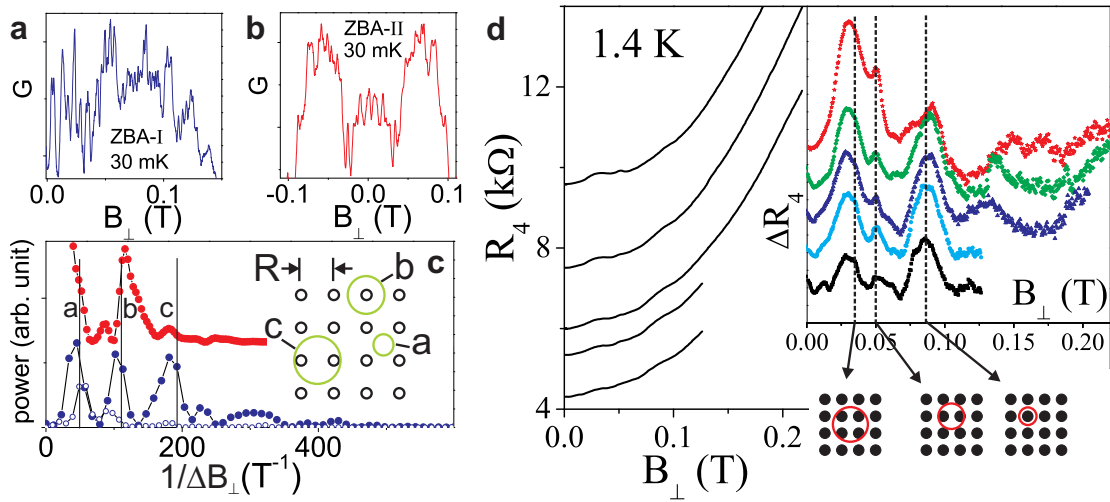


FIG. 2: Quantum and classical magnetotransport in perpendicular magnetic field (B_{\perp}). Typical linear magnetoconductance oscillation at **a**, a single-peak resonance (ZBA-I), and **b**, a double-peak resonance (ZBA-II). **c**, Power spectra of the magnetoconductance oscillations. The filled markers (blue: ZBA-I and red: ZBA-II) represent spectra obtained from the range $|B_{\perp}| \leq 0.065$ T, while the empty (blue) marker represents the spectrum (vertically scaled for clarity) from 0.065 T $< B_{\perp} < 0.15$ T. The orbits corresponding to the peaks are indicated in the schematic. **d**, Four-probe linear magnetoresistance at 1.4 K for five electron densities from 1.22 (topmost trace) to 1.39×10^{10} cm^{-2} (bottom trace), where well-defined ZBA's appear at low temperatures. Inset: Magnetoresistance after subtracting the parabolic background. The dashed lines, which denote various commensurate orbits, are computed using the average density of 1.31×10^{10} cm^{-2} , and $R \approx 500$ nm.

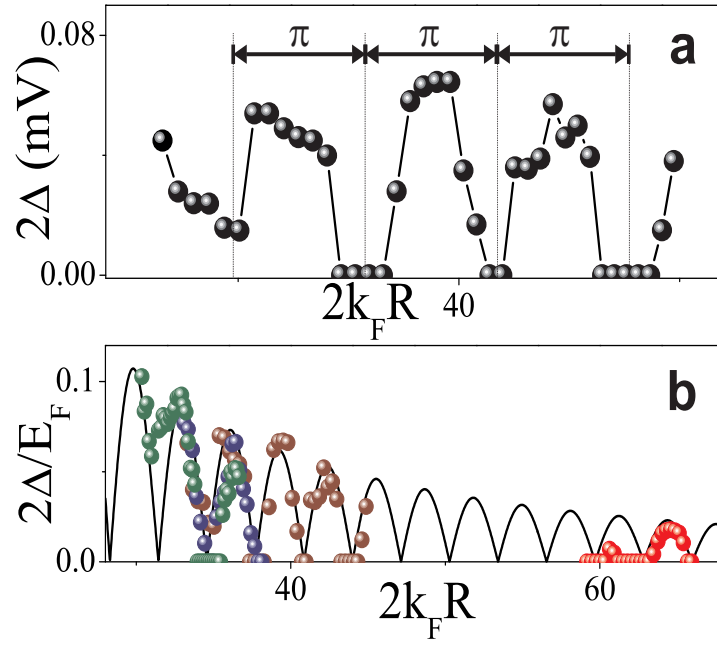
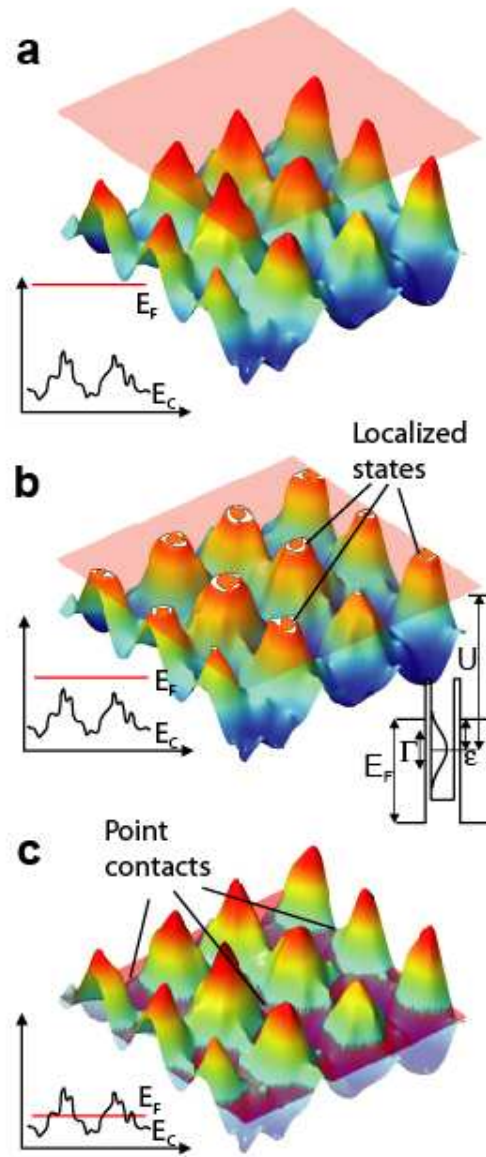
Siegert *et al.*

FIG. 3: RKKY indirect exchange and “ $2k_F R$ -oscillations”: **a**, 2Δ from Fig. 1c as a function $2k_F R$, where k_F is the Fermi wave vector, and R is the inter-spin distance obtained from magnetoconductance oscillations. **b**, $2\Delta/E_F$ as a function of $2k_F R$ for four different devices. Solid line is proportional to the pairwise RKKY range function (see text). Local disorder governs the experimentally attainable range of $2k_F R$ within a given mesoscopic device.



Siegert et al.

FIG. 4: Schematic of background disorder and local moment formation. While the rapid fluctuations arise from dopant density fluctuations, the slow quasi-regular fluctuations indicates effect of strong correlation in the donor layer at large filling. **a**, large, **b**, intermediate, and **c**, low, carrier density regimes are shown. Our experimental results conform to the island-in-sea scenario of Fig. 4b.